Dynamics of a vapor nanobubble collapsing near a solid boundary

2015 J. Phys.: Conf. Ser. 656 012012

(http://iopscience.iop.org/1742-6596/656/1/012012)

Journal of Physics: Conference Series **656** (2015) 012012 doi:10.1088/1742-6596/656/1/012012

Dynamics of a vapor nanobubble collapsing near a solid boundary

Francesco Magaletti, Mirko Gallo, Luca Marino, Carlo Massimo Casciola

Dipartimento di Ingegneria Meccanica e Aerospaziale, Università di Roma "La Sapienza", via Eudossiana 18, 00184 Roma Italy

E-mail: carlomassimo.casciola@uniroma1.it

Abstract. In the present paper a diffuse interface approach [1] is used to address the collapse of a sub-micron vapor bubble near solid boundaries. This formulation enables an unprecedented description of interfacial flows that naturally takes into account topology modification and phase changes (both vapor/liquid and vapor/supercritical fluid transformations). Results from numerical simulations are exploited to discuss the complex sequence of events associated with the bubble collapse near a wall, encompassing shock-wave emissions in the liquid and reflections from the wall, their successive interaction with the expanding bubble, the ensuing asymmetry of the bubble and the eventual jetting phase.

1. Introduction

The collapse of vapor bubbles near solid boundaries started being investigated in the last century, motivated by the destructive effects of cavitation on ship propellers and hydraulic turbines and pumps and is still today receiving an increasingly significant attention [2, 3, 4]. Only recently the increasing impact of the micro and nano technologies shifted the attention from millimeter-sized to micrometer or sub-micrometer bubbles. In a *lab on a chip*, cavitation can be employed for microfluidic pumping [5], to enhance mixing and for surface cleaning purposes [6]. Cavitation is also exploited in medicine, e.g. in high intensity focused ultrasound (HIFU) and extracorporeal shock wave lithotripsy (ESWL) [7] to enhance drug delivery or localized heat deposition deep within the body, and to induce cell membrane poration [8] or to comminute kidney stones [9].

The cornerstone work of Rayleigh [10], refined in [11, 12, 13, 14, 15], is still today impressive for the correspondence with experimental results despite substantial simplifying assumptions. Successively, nearby boundaries were addressed by numerical simulations [16, 17, 18].

In the present paper, by extending the analysis of symmetric bubble collapse discussed in [1], we use the diffuse interface approach to address the collapse of a sub-micron vapor bubble near solid boundaries. This formulation enables a natural description of interfacial flows, changes of topology, and vapor/liquid and vapor/supercritical fluid phase changes which have been shown to be crucial for the correct description of the final stages of the bubble collapse.

2. Mathematical model

We exploit an unsteady diffuse interface description [19, 1] of the two-phase (liquid/vapor) flow in a domain $\mathcal{D}$ based on the van der Waals gradient approximation of the free energy functional

$F[\rho,\theta]$ [20]:

$$F[\rho,\theta] = \int_{\mathcal{D}} \hat{f} dV = \int_{\mathcal{D}} \left(\hat{f}_0 \left(\rho,\theta\right) + \frac{\lambda}{2} |\boldsymbol{\nabla}\rho|^2 \right) dV \,,$$

where $\hat{f} = \hat{f}_0 + \lambda/2|\nabla\rho|^2$ with $\hat{f}_0\left(\rho,\theta\right)$ the classical Helmholtz free energy density per unit volume of the homogeneous fluid at temperature θ and mass density ρ. Together with $\hat{f}_0$, the coefficient $\lambda(\rho,\theta)$ embodies all the information on the interfacial properties of the liquid-vapor system, namely surface tension σ and interface thickness ϵ. For a van der Waals fluid, the free energy reads

$$\hat{f}_0\left(\rho,\theta\right) = \bar{R}\rho\theta \left[-1 + \log\left(\frac{\rho\, K\, \theta^{1/\delta}}{1-b\rho} \right) \right] - a\rho^2 \,,$$

with $\delta = \bar{R}/c_v$, $\bar{R}$ the gas constant, c_v the constant volume specific heat, a and b the van der Waals coefficients and K a constant related to the de Broglie length [21].

The dynamics of the inhomogeneous system is described by the equations for mass ρ, momentum $\rho\mathbf{u}$, and total energy density $E = 1/2\rho|\mathbf{u}|^2 + \mathcal{U}$, with $\mathcal{U} = \bar{R}\theta/\delta - a\rho + \lambda|\boldsymbol{\nabla}\rho|^2/(2\rho)$ the internal energy density,

$$\frac{\partial \rho}{\partial t} + \boldsymbol{\nabla}\cdot(\rho\mathbf{u}) = 0 \,,$$

$$\frac{\partial \rho\mathbf{u}}{\partial t} + \boldsymbol{\nabla}\cdot(\rho\mathbf{u}\otimes\mathbf{u}) = \boldsymbol{\nabla}\cdot\boldsymbol{\tau} \,,$$

$$\frac{\partial E}{\partial t} + \boldsymbol{\nabla}\cdot(\mathbf{u}E) = \boldsymbol{\nabla}\cdot\left[\boldsymbol{\tau}\cdot\mathbf{u} - \mathbf{q_e}\right] \,.$$

This system of conservation equations is closed with thermodynamically consistent constitutive relations for the stress tensor $\boldsymbol{\tau}$ and the energy flux $\mathbf{q_e}$. Under the assumptions of local equilibrium and linear dependence of thermodynamic fluxes on thermodynamic forces – $\boldsymbol{\nabla}\theta$ and $\boldsymbol{\nabla}\mathbf{u}$ – the general approach outlined in [22] leads to identify the stress tensor as

$$\boldsymbol{\tau} \;=\; \left(-p_0 + \frac{\lambda}{2}|\boldsymbol{\nabla}\rho|^2 + \rho\boldsymbol{\nabla}\cdot(\lambda\boldsymbol{\nabla}\rho) \right)\boldsymbol{I} - \lambda\boldsymbol{\nabla}\rho\otimes\boldsymbol{\nabla}\rho + \mu\left[\left(\boldsymbol{\nabla}\mathbf{u} + \boldsymbol{\nabla}\mathbf{u}^T\right) - \frac{2}{3}\boldsymbol{\nabla}\cdot u\boldsymbol{I} \right] \,,$$

where the usual viscous terms with $\mu > 0$ in the last term are the source of irreversibility (the second viscosity coefficient is assumed to be $-2\mu/3$). From the van der Waals free energy density $\hat{f}_0$, Eq. (1), the pressure is $p_0 = \bar{R}\rho\theta/(1-b\rho) - a\rho^2$. Concerning the energy flux, one finds

$$\mathbf{q_e} = \lambda\rho\boldsymbol{\nabla}\rho\boldsymbol{\nabla}\cdot\mathbf{u} - k\boldsymbol{\nabla}\theta \,,$$

where $k > 0$ is the thermal conductivity. We like to stress that the adoption of a consistent thermodynamic model, like the van der Waals fluid, embodies the model with all the features related to phase change, i.e. latent heat release/adsorption during condensation/vaporization and transition to supercritical conditions at increasing temperature and pressure.

3. Results and discussion

The simulations are performed using an axisymmetric code that is the extension of the one developed to deal with the spherically symmetric case, see [1] for details on the numerical technique. The system, consisting of a pure van der Waals fluid, is initialized with a vapor bubble of radius R_{eq} centered at z_0, the distance between the planar wall and the bubble center. The vapor bubble is in equilibrium with the confining liquid at temperature $\theta/\theta_c = 0.6$, with θ_c the critical temperature of the fluid. A shock wave with intensity $I = (p_2 - p_1)/p_1$, with p_2 and

p_1 the pressure in the perturbed and the unperturbed state, respectively, is initialized in the liquid phase to propagate toward the wall and hit the bubble, thus triggering its collapse. The fluid domain with dimension $4R_{eq} \times 4R_{eq}$ is discretized with a uniform grid 2048×2048. The dimensionless parameters of the simulations are $Re = R_{eq}\sqrt{p_c\rho_c}/\mu = 50$, $Pr = 3\mu\bar{R}/(8k) = 0.2$, and $\mathcal{C} = \lambda\rho_c^2/(p_c R_{eq}^2) = 1.6 \times 10^{-4}$, which correspond, e.g., to a bubble radius order 100 nm with typical viscosity, thermal conductivity, surface tension and critical values of water.

In our simulations we invariably observe bubble rebounds induced by the vapor temperature raise inside the cavity which, during collapse, exceeds the critical temperature to form an incondensable phase. This feature was most unexpected when first observed during numerical experiments of spherical collapse of a pure vapor nanobubble [1]. Two examples of the evolution are represented in Fig. 1 for two different initial wall distances, when the collapse is triggered by a shock wave with intensity $I = 75$. The relatively weak impinging shockwave is not sufficient to immediately break the spherical symmetry and to produce the classical liquid jet that porates the bubble, as observed in millimeter-bubble experiments [23, 24, 6, 4]. At sub-micron scale the surface tension is, in fact, predominant and preserves the nearly spherical shape during the first part of the evolution. Symmetry breaking eventually occurs when the bubble shrinks to its minimum volume and a non-spherical shockwave is emitted. This effect is more pronounced for bubbles closer to the wall. In these conditions the shockwave produced at collapse consists

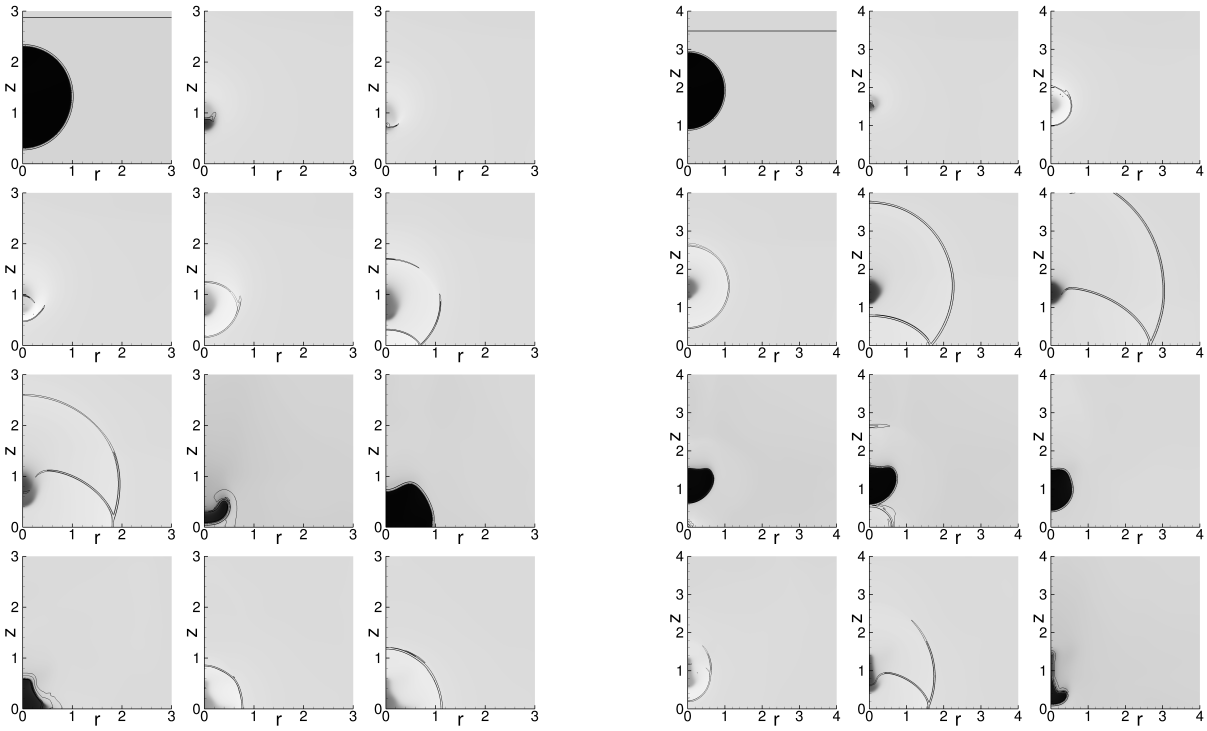

Figure 1. Snapshots during the evolution of a collapsing bubble with $z_0 = 1.3$ (left) and $z_0 = 1.9$ (right). The sequence runs from left to right and from top to bottom and is not uniformly spaced in time (left: $t = 0, 1.887, 1.907, 1.923, 1.953, 2.004, 2.131, 3.502, 5.403, 6.303, 6.480, 6.524$; right: $t = 0, 1.911, 1.956, 2.023, 2.202, 2.337, 3.833, 3.902, 5.937, 6.353, 6.524, 7.997$). The grey tones from darker to lighter represent the density field from smaller (vapor phase) to higher (liquid phase). The black lines are Schlieren-like iso-lines obtained as $S = \exp(-|\boldsymbol{\nabla} p_0|/|\boldsymbol{\nabla} p_0|_{max})$. The drawn iso-levels are $S = 0.9$ and $S = 1$ in order to highlight the regions with the highest pressure gradients, i.e. the vapor-liquid interface and the shockwaves.

of two curved shock fronts that propagate toward and away from the wall, respectively. The former is eventually reflected by the solid wall and interacts back with the re-expanding bubble. During this stage the bubble flattens out and moves toward the wall. The expansion stage is strongly affected by the bubble–wall distance, with the closest one (left panel in Fig. 1) touching the wall and the farthest one (right panel in Fig. 1) remaining detached. During the bubble expansion, the liquid in the thin layer between vapor and wall is compressed and a new shockwave is observed, plots in the third row on the right of Fig. 1. This sequence of bubble–wall interactions completely breaks the spherical symmetry, thereby reducing the strength of the successive collapse. Eventually, the field becomes more and more complex, until dissipation prevails.

For stronger shocks the nanobubble becomes asymmetric much earlier, originating a strong jet focused towards the walls. A complete simulation campaign is presently under way to investigate the role of the different parameters entering the problem, focusing in particular on the pressure pulse induced at the wall during the collapse, a major concern in most applications of collapsing micro/nano bubbles. A further crucial parameter is the maximum achieved temperature which, according to our preliminary results, typically ranges between 5 and 15 times the critical temperature and is strongly depend on the specific initial conditions.

The present results preliminarily confirm that the thermodynamically consistent description of cavitation bubbles provided through the diffuse interface model we have briefly outlined above allows to follow in full detail the complex dynamics and thermodynamics of the non-spherical collapse, accounting for changes of topology in the bubble. More work is under way to include additional features to the model, like chemical effects related to molecular dissociation and ionization and the presence of dissolved gas in the otherwise pure liquid.

References

[1] Magaletti F, Marino L and Casciola C 2015 *Physical Review Letters* **114** 064501
[2] Silberrad D 1912 *Engineering* 33–35
[3] Leighton T 2012 *The acoustic bubble* (Academic press)
[4] Obreschkow D, Tinguely M, Dorsaz N, Kobel P, de Bosset A and Farhat M 2011 *Physical Review Letters* **107**(20) 204501
[5] Dijkink R and Ohl C D 2008 *Lab on a Chip* **8** 1676–1681
[6] Ohl C D, Arora M, Dijkink R, Janve V and Lohse D 2006 *Applied Physics Letters* **89** 074102
[7] Coussios C C and Roy R A 2008 *Annu. Rev. Fluid Mech.* **40** 395–420
[8] Sankin G, Yuan F and Zhong P 2010 *Physical Review Letters* **105** 078101
[9] Zhu S, Cocks F H, Preminger G M and Zhong P 2002 *Ultrasound in Medicine & Biology* **28** 661–671
[10] Rayleigh L 1917 *The London, Edinburgh, and Dublin Philosophical Magazine and Journal of Science* **34** 94–98
[11] Keller J B and Kolodner I I 1956 *Journal of Applied Physics* **27** 1152–1161
[12] Hickling R and Plesset M S 1964 *Physics of Fluids (1958-1988)* **7** 7–14
[13] Plesset M S and Chapman R B 1971 *Journal of Fluid Mechanics* **47** 283–290
[14] Plesset M S and Prosperetti A 1977 *Annual Review of Fluid Mechanics* **9** 145–185
[15] Shima A and Sato Y 1981 *Journal de Mecanique* **20** 253–271
[16] Blake J R and Gibson D 1981 *Journal of Fluid Mechanics* **111** 123–140
[17] Tipton R E, Steinberg D J and Tomita Y 1992 *Jsme International Journal. Ser. 2, Fluids Engineering, Heat Transfer, Power, Combustion, Thermophysical Properties* **35** 67–75
[18] Ding Z and Gracewski S 1996 *Journal of Fluid Mechanics* **309** 183–209
[19] Anderson D, McFadden G and Wheeler A 1998 *Annual Review of Fluid Mechanics* **30** 139–165 ISSN 0066-4189
[20] Jamet D, Lebaigue O, Coutris N and Delhaye J 2001 *Journal of Computational Physics* **169** 624–651
[21] Zhao N, Mentrelli A, Ruggeri T and Sugiyama M 2011 *Physics of Fluids* **23** 086101
[22] De Groot S R and Mazur P 2013 *Non-equilibrium thermodynamics* (Courier Dover Publications)
[23] Benjamin T B and Ellis A T 1966 *Philosophical transactions of the Royal Society of London. Series A, Mathematical and physical sciences* **260** 221–240
[24] Lauterborn W and Bolle H 1975 *Journal of Fluid Mechanics* **72** 391–399